JOURNAL OF AIRCRAFT
Vol. 40, No. 2, March–April 2003

Parallelized Three-Dimensional Unstructured Euler Solver for Unsteady Aerodynamics

Erdal Oktay*
Roketsan, Missiles Industries, Inc., 06780 Ankara, Turkey
and
Hasan U. Akay† and Ali Uzun‡
Indiana University—Purdue University Indianapolis, Indianapolis, Indiana 46202

A parallel algorithm for the solution of unsteady Euler equations on unstructured and moving meshes is developed. A cell-centered finite volume scheme is used. The temporal discretization involves an implicit time-integration scheme based on backward-Euler time differencing. The movement of the computational mesh is accomplished by means of a dynamically deforming mesh algorithm. The parallelization is based on decomposition of the domain into a series of subdomains with overlapped interfaces. The scheme is computationally efficient, time accurate, and stable for large time increments. Detailed descriptions of the solution algorithm are given, and computations for airflow around a NACA0012 airfoil and a missile configuration are presented to demonstrate the applications.

Nomenclature

a	=	speed of sound
$\boldsymbol{a}$	=	acceleration vector
C_N	=	normal force coefficient
C_p	=	pressure coefficient
d	=	missile diameter
e	=	total energy per unit volume
$\boldsymbol{F}$	=	flux vector
k	=	reduced frequency
L	=	axial missile length
M	=	Mach number
$\boldsymbol{n}$	=	surface normal unit vector
p	=	pressure
$\boldsymbol{Q}$	=	vector of conservation variables
$\boldsymbol{R}$	=	residual vector
S_p	=	speed up
t	=	time
u, v, w	=	velocity components in x, y, and z directions, respectively
V	=	volume
$\boldsymbol{V}$	=	flow velocity vector
$\boldsymbol{W}$	=	mesh velocity vector
W_n	=	contravariant face speed
x, y, z	=	Cartesian coordinates
α	=	angle of attack, deg
γ	=	specific heats ratio
ρ	=	density
ω	=	frequency

Subscripts

c	=	cell-centered value
n	=	normal direction
w	=	wall value
x, y, z	=	Cartesian components
∞	=	freestream condition

Introduction

ACCURATE and fast prediction of unsteady flow phenomena for practical applications in aerodynamics still remains to be a challenging problem because of excessive computer resources needed for problems involving complex geometries and large computational domains. Although the compressible Navier–Stokes equations with appropriate turbulence models provide the most accurate solution for aerodynamic characteristics of moving bodies, the solution is prohibitively expensive because of the need for very high mesh densities requiring several millions of mesh points, which have to be solved several thousand times, if not more. Unsteadiness in flow conditions and moving nature of the bodies involved make the solution expensive and time consuming. Hence, there is a need for simplifications and more innovative techniques for real-life applications. Euler equations, in which the viscosity of the fluid is neglected as a first approximation to the Navier–Stokes equations, give valuable information on aerodynamic force and moment characteristics of bodies at moderate angles of attacks. As an attempt to develop a practical tool for prediction of aerodynamic features of missiles in flight, the authors in this paper present a transient Euler solver that uses a time-accurate implicit solver for the solution of transient phenomena and a deforming mesh approach for the movements of the body. Following the experience gained in Uzun et al.,[1] the solver is parallelized using a domain-decomposition approach by subdividing the flow domain into unstructured subdomains and overlapped interfaces. This enables the code to run faster on network of PCs and workstations. The previously developed serial Euler solver, USER3D,[2] has been modified to add these features for solving unsteady aerodynamics and moving body problems. Validation of the serial version of the code for steady-state problems has been documented elsewhere.[3,4] The present algorithm is based on an implicit, cell-centered finite volume formulation. For upwinding, the fluxes on cell faces are obtained using Roe's flux-difference splitting method because of its superior shock-detection and antidissipative features.[5] The dynamically deforming mesh algorithm that is coupled with the flow solver moves the computational mesh to conform to body movements. For instantaneous positions of the

Presented as Paper 2002-0107 at the AIAA 40th Aerospace Sciences Meeting and Exhibit, Reno, NV, 14–17 January 2002; received 2 April 2002; revision received 20 November 2002; accepted for publication 2 December 2002.

*Manager, Aerodynamics Department, Elmadag. Member AIAA.
†Professor and Chair, Department of Mechanical Engineering. Senior Member AIAA.
‡Graduate Student, Department of Mechanical Engineering, Purdue University, West Lafayette, Indiana.

moving boundary, the solution of a dynamically deforming spring network at each time step is updated with an implicit algorithm that uses the linearized backward-Euler time-differencing scheme.

In this paper, following the discussion of the developed algorithms, the validation of the code with experiments using an unsteady NACA0012 airfoil test case as a first benchmark is presented. Features of the developed algorithms for time-accurate prediction of unsteady normal force characteristics are demonstrated on a missile geometry next. A new method for prediction of aerodynamic dynamic stability derivatives using the present algorithms is presented in Ref. 6.

Flow Solver

Euler Equations

Flows around oscillating bodies can be solved either by using relative coordinates attached to the body[7] or an arbitrary Lagrangian–Eulerian (ALE) approach[8] on meshes that move and deform continuously with the movement of the body. The use of a relative coordinate system for a single-body problem is relatively simple, and it eliminates the need for mesh movements. However, for multibodies moving independently this requires separate computational mesh patches and relative coordinate systems attached to each body, where the flux balances between patches are achieved via interpolations as in Chimera schemes.[9] With the ALE/deforming mesh approach, on the other hand, both singlebody and multibody systems can be solved by using the same computational mesh and coordinate system. Although this approach is restricted to moderate movements of the bodies, large movements can be treated by introducing new meshes at selected intervals of the movements. In this paper the ALE formulation with moving/deforming features has been used. The three-dimensional unsteady and inviscid flow equations for a finite-volume cell in ALE form are expressed in the following form (e.g., see Singh et al.[10]):

$$\frac{\partial}{\partial t}\iiint_{\Omega} \boldsymbol{Q}\,\mathrm{d}V + \iint_{\partial\Omega} \boldsymbol{F}\cdot\boldsymbol{n}\,\mathrm{d}S = 0 \tag{1}$$

where $\boldsymbol{Q} = [\rho, \rho u, \rho v, \rho w, e]^T$ is the vector of conserved flow variables,

$$\boldsymbol{F}\cdot\boldsymbol{n} = [(\boldsymbol{V}-\boldsymbol{W})\cdot\boldsymbol{n}]\begin{bmatrix}\rho\\ \rho u\\ \rho v\\ \rho w\\ e+p\end{bmatrix} + p\begin{bmatrix}0\\ n_x\\ n_y\\ n_z\\ W_n\end{bmatrix} \tag{2}$$

is the convective flux vector; $\boldsymbol{n} = n_x\boldsymbol{i} + n_y\boldsymbol{j} + n_z\boldsymbol{k}$ is the normal vector to the boundary $\partial\Omega$; $V = u\boldsymbol{j} + v\boldsymbol{j} + w\boldsymbol{k}$ is the fluid velocity; $\boldsymbol{W} = \boldsymbol{i}\partial x/\partial t + \boldsymbol{j}\partial y/\partial t + \boldsymbol{k}\partial z/\partial t$ is the mesh velocity; and $W_n = \boldsymbol{W}\cdot\boldsymbol{n} = n_x\partial x/\partial t + n_y\partial y/\partial t + n_z\partial z/\partial t$ is the face speed of finite volume cells in the normal direction. The pressure p is given by the equation of state for a perfect gas:

$$p = (\gamma-1)\left[e - \tfrac{1}{2}\rho(u^2+v^2+w^2)\right] \tag{3}$$

These equations have been nondimensionalized by the freestream density ρ_∞, the freestream speed of sound a_∞, and a reference length. The domain of interest is divided into a finite number of tetrahedral cells, and Eq. (1) is applied to each cell in a cell-centered fashion (e.g., see Frink et al.[11]).

Boundary Conditions

For subsonic inflow and outflows the characteristic boundary conditions are applied using Riemann invariants. For supersonic inflow the known values of conservation variables are specified. For supersonic outflows the values of conservation variables are extrapolated from inside the flow domain. For moving boundaries the wall boundary conditions are modified by taking the mesh movements into account. Thus, the flow tangency condition is imposed by calculating the flow velocity on solid walls from

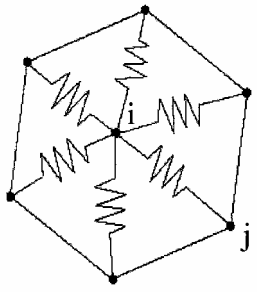

Fig. 1 Spring analogy around a mesh point in deforming mesh algorithm.

$$\boldsymbol{V}_w = \boldsymbol{V}_c - \boldsymbol{n}\cdot[(\boldsymbol{V}-\boldsymbol{W})\cdot\boldsymbol{n}] \tag{4}$$

The wall pressure is calculated from the normal momentum equation as

$$\frac{\partial p}{\partial n} = -\rho\boldsymbol{n}\cdot\boldsymbol{a}_w \tag{5}$$

The preceding boundary conditions reduce to steady flow conditions by setting the mesh velocity $\boldsymbol{W}$ to zero.

Deforming Mesh Algorithm

The deforming mesh algorithm models the unsteady aerodynamic response that is caused by the forced oscillations of a configuration. Hence, the mesh movement is known beforehand. The algorithm used in this study has been previously developed by Batina.[12] In this algorithm the computational mesh is moved to conform to the instantaneous position of the moving boundary at each time step. The algorithm treats the computational mesh as a system of interconnected springs at every mesh point constructed by representing each edge of every cell by a linear spring as shown schematically in Fig. 1 for a two-dimensional configuration. The spring stiffness for a given edge $i-j$ is taken as inversely proportional to the length of the edge as follows:

$$k_m = 1\Big/\sqrt{(x_j-x_i)^2 + (y_j-y_i)^2 + (z_j-z_i)^2} \tag{6}$$

The mesh points on the outer boundary of the domain are held fixed while instantaneous location of the points on the inner boundary (i.e., moving body) is given by the body motion. At each time step the static equilibrium equations in the x, y, and z directions that result from a summation of forces are solved iteratively using Jacobi iterations at each interior node i of the mesh for the displacements Δx_i, Δy_i, and Δz_i.

After the new locations of the nodes are found, the new metrics (i.e., new cell volumes, cell face areas, face normal vectors, etc.) are computed. The nodal displacements are divided by the time increment to determine the velocity of the nodes. It is assumed that the velocity of a node is constant in magnitude and direction during a time step. Once the nodal velocities are computed, the velocity of a triangular cell face is found by taking the arithmetic average of the velocities of the three nodes that constitute the face. The face velocities are used in the flux computations in the solution algorithm.

Geometric Conservation

Because of mesh movements, a geometric conservation law has to be solved in addition to the mass, momentum, and energy conservation laws. This law is expressed in integral form as (e.g., see Batina[12]):

$$\frac{\partial}{\partial t}\iiint_{\Omega} \mathrm{d}V + \iint_{\partial\Omega} \boldsymbol{W}\cdot\boldsymbol{n}\,\mathrm{d}S = 0 \tag{7}$$

This geometric conservation law provides a self-consistent solution for the local cell volumes and is solved using the same scheme used for all other flow conservation equations.

Time Integration

A cell-centered finite volume formulation is employed. The flow variables are volume-averaged values; hence, the governing equations are rewritten in the following form:

$$\Delta \boldsymbol{Q}^n \frac{V^{n+1}}{\Delta t} = -\iint_{\partial\Omega} \boldsymbol{F}(\boldsymbol{Q}) \cdot \boldsymbol{n}\, \mathrm{d}S - \boldsymbol{Q}^n \frac{\Delta V^n}{\Delta t} \tag{8}$$

where $\Delta \boldsymbol{Q}^n = \boldsymbol{Q}^{n+1} - \boldsymbol{Q}^n$, V^n is the cell volume at time step n, V^{n+1} is the cell volume at time step $n+1$, $\Delta V^n = V^{n+1} - V^n$, and Δt is the time increment.

Because an implicit time-integration scheme is employed, fluxes are evaluated at time step $n+1$. The integrated flux vector is linearized according to

$$\boldsymbol{R}^{n+1} = \boldsymbol{R}^n + \frac{\partial \boldsymbol{R}^n}{\partial \boldsymbol{Q}^n} \Delta \boldsymbol{Q}^n \tag{9}$$

Hence the following system of linear equations is solved at each time step:

$$\boldsymbol{A}^n \Delta \boldsymbol{Q}^n = \boldsymbol{R}^n - \boldsymbol{Q}^n (\Delta V^n / \Delta t) \tag{10}$$

where

$$\boldsymbol{A}^n = \frac{V^n}{\Delta t} \boldsymbol{I} - \frac{\partial \boldsymbol{R}^n}{\partial \boldsymbol{Q}^n} \tag{11}$$

$$\boldsymbol{R}^n = -\iint_{\partial\Omega} \boldsymbol{F}(\boldsymbol{Q})^n \cdot \boldsymbol{n}\, \mathrm{d}S \tag{12}$$

The flow variables are stored at the centroid of each tetrahedron. Flux quantities across cell faces are computed using Roe's flux-difference splitting method for upwinding because of its superior shock-detection and antidissipative features.[5]

The implicit time-integration method used in this study has been previously suggested by Anderson[13] for the solution of steady-state Euler equations on stationary meshes. The system of simultaneous equations that results from the application of Eq. (10) for all of the cells in the mesh can be obtained by a direct inversion of a large matrix with large bandwidth. However, the direct inversion technique demands a huge amount of memory and extensive computer time to perform the matrix inversions for three-dimensional problems. Instead, a Gauss–Seidel relaxation procedure with 5×5 submatrices $\boldsymbol{A}^n$ for the five conservation variables in each cell is used for the solution of the system of equations. In this relaxation scheme the solution is obtained through a sequence of iterations in which an approximation of $\Delta \boldsymbol{Q}^n$ is continually refined until acceptable convergence is reached.

Parallelization of the Code

For parallelization of the code, a domain-decomposition approach is used, where the flow domain is subdivided into a number of subdomains equal or more than the number of available processors. The subdomains, also named *solution blocks*, are interconnected by means of interfaces, which are of matching and overlapping type, following the methodology proposed in Akay et al.[14] Overlaps are of one cell between two blocks. The interfaces serve to exchange the data between the blocks. The schematic in Fig. 2 shows the arrangement for a case of two neighboring blocks. Each block has both a block solver and an interface solver. The governing equations for flow or mesh movements are solved in a block solver, which updates its interface solver with newly calculated nodal variables at each iteration step. The interface solver in each block, in turn, communicates with the interface solver of the neighboring block for the same interface. Each interface solver also updates its block after receiving information from its neighbor. In each block the nodes on the interfaces are flagged as either receiving or sending nodes. The ones on the interior side of the blocks are sending nodes, and the ones on the exterior side are receiving nodes. The sending nodes send their data to the corresponding nodes in the neighboring blocks, and

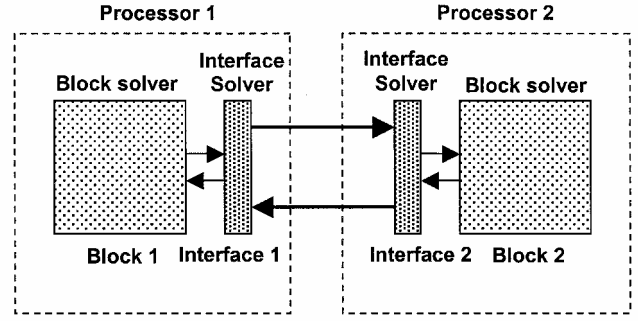

Fig. 2 Block and interface solvers for block-to-interface and interface-to-interface communications.

the receiving nodes receive the data from the corresponding nodes in the neighboring block. The communication between the blocks is achieved by means of the message-passing interface (MPI).[15] Both the flow and mesh deformation solvers are parallelized using the same algorithm.

Mesh Partitioning for Parallelization

The computational domain that is discretized with an unstructured mesh is partitioned into subdomains or blocks using a program named General Divider, which is a general unstructured mesh-partitioning code developed at the CFD Laboratory at Indiana University—Purdue University Indianapolis.[16] It is capable of partitioning both structured (hexahedral) and unstructured (tetrahedral) meshes in three-dimensional geometries. The interfaces between partitioned blocks are of matching and overlapping type. The interfaces serve to exchange data among the blocks.[14]

Structure of the Parallel Code

The following steps are involved in the parallelization:

1) The computational domain Ω is divided into blocks $\Omega_i (i = 1, \ldots, n)$, where $n \geq p$ is the number of blocks and p is the number of processors. The General Divider program is used to partition the domain into blocks.

2) Interfaces with one element overlap are assigned between neighboring blocks. This is also done by the General Divider program.

3) The block and interface information are provided to the parallel USER3D program.

4) Blocks are distributed to different machines on the network. Depending on the availability of the processors vs the number of blocks, one or more blocks might be assigned to each processor.

5) Both the mesh movement and the unsteady Euler equations are solved in block solvers for unsteady moving boundary problems. Only the steady Euler equations are solved in block solvers in the case of steady-state problems.

6) Interface information is exchanged between neighboring blocks in interface solvers.

The main differences between the steady and the unsteady flow solution schemes are as follows:

1) The dynamically deforming mesh algorithm is only used in unsteady flow problems. It is not needed in steady-state computations because the computational mesh remains stationary in steady-state problems.

2) Local time-stepping strategy accelerates the convergence to steady state; hence, this strategy is used often while solving steady-state problems.

3) For unsteady problems a global time increment is used because the unsteady flow solution has to be time accurate. All cells in the computational mesh use the same time increment during the course of unsteady flow computations.

4) For both steady and unsteady problems the flow solver performs 20 Gauss–Seidel iterations in each time step to solve the system of equations. Because time accuracy is not desired in steady-state problems, the flow solver first performs the 20 iterations and then communicates once in each time cycle while solving steady-state

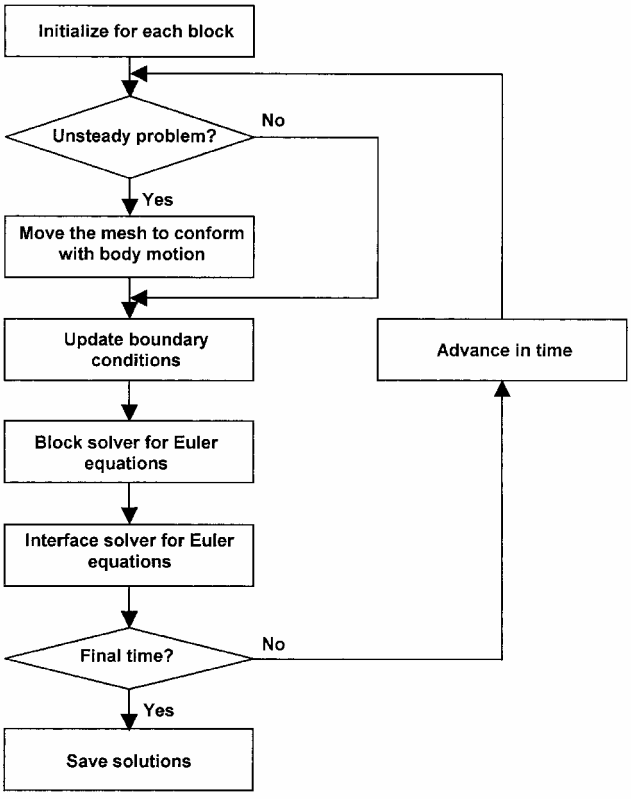

Fig. 3 Flowchart of the parallel algorithm.

problems. This approach reduces the communication time requirements of the flow solver while solving steady-state problems.

5) In unsteady problems both the flow and deforming mesh solvers communicate once after every iteration within each time step. If this is not done, errors are introduced into the solution as a result of parallelism.

A general flowchart of the preceding algorithms is given in Fig. 3.

Test Cases

Two tests cases have been considered here to illustrate various features of the developed algorithms. The program was first tested for accuracy by considering a well-known oscillating case for the NACA0012 airfoil. The unsteady results were compared with the experimental and other numerical results in the literature. The time accuracy of the results was verified with multiple blocks and different meshes and time step sizes. To demonstrate the applicability of the current method to complex problems and to study the parallel efficiency of the developed algorithms, a basic-missile configuration has been considered as the second test case. Both steady and unsteady computations have been performed.

In all cases a steady-state solution was first obtained to be used as an initial condition for the unsteady calculations to follow. A local time-stepping approach was used for steady calculations with the local time step in each cell m determined from the condition:

$$\Delta t_m \leq CFL(V_m/A_m) \tag{13}$$

where CFL is the Courant–Friedrichs–Lewy number, V_m is the cell volume, and

$$A_m = \sum_{i=1}^{3} \left[\left(\left| u_i^m \right| + a_m \right) S_i^m \right] \tag{14}$$

where u_m^i is the ith direction flow speed in cell m, a_m is the speed of sound in cell m, and S_i^m is the projected area of the cell m in the ith coordinate direction. Steady iterations typically start at $CFL = 5$, which is linearly increased up to 20–50 range within 50 time steps or so, and solutions continue until the residuals drop three orders of magnitude—typically within 200–400 steps. A constant time-step value is used for all unsteady calculations, with the time step determined from the duration of unsteady cycles. The time-step size needed for unsteady flows depends on the mesh density and the speed of unsteady oscillations. For each time step 20 Gauss–Seidel iterations are performed for the solution of flow equations in each solution block. Although the interface data are exchanged at every iteration, in each step of the unsteady calculations they are exchanged only at the end of 20 iterations in steady cases. The deforming mesh solver, needed for each time step of the unsteady calculations, also exchanges interface information among blocks during the Jacobi iterations of the spring assembly equations. Hence, substantially extra amount of communication is needed in each step of the unsteady calculations, because of extra information exchange needed in both flow and deforming mesh solvers.

The unstructured meshes used here were generated using the mesh generation module of a commercially available finite element CAD package I-DEAS™. All cases were run on Indiana University's IBM RISC 6000/SP POWER3/Thin Node multiprocessor system, with 375-MHz clock cycle CPU and 2–4 GB memory processors. A maximum of 20 processors were allocated for this project.

NACA0012 Airfoil Case

This well-documented basic case was tested by Landon[17] under sinusoidal pitching oscillations at different frequencies. For the conditions considered here, the angle of attack varies about the quarter-chord with amplitude α_p as

$$\alpha(t) = \alpha_m + \alpha_p \sin(\omega_\alpha t) \tag{15}$$

where $\alpha_m = 0.016$ deg is the mean angle of pitching; $\alpha_p = 2.51$ deg is the amplitude of pitching; $\omega_\alpha = 2kV_\infty/c$ is the frequency of pitching oscillations; $k = 0.0814$ is the reduced frequency; $c = 1$ the airfoil chord length; t is the nondimensional time; and V_∞ is the freestream velocity, with $M_\infty = 0.755 = V_\infty/a_\infty$ as the freestream Mach number.

The steady-state solution at the mean angle of pitching position was used as an initial solution to the unsteady calculations. The solutions were computed using two meshes: the coarse mesh consisting of 11,448 cells and 2859 nodes, and the fine mesh consisting of 99,884 cells and 20,941 nodes. Both meshes were partitioned into various number of blocks from 2 through 20 for parallel computing. Shown in Figs. 4a and 4b are the plots of the partitioned meshes in the vicinity of the airfoil at maximum and minimum angle of attack positions, respectively, for the 20-block and fine-mesh case. Overlapped interfaces common to each neighboring block are indicated with darker lines. Because of two-dimensional nature of the problem, one layer of cells is used in the out-of-plane directions, with the symmetry boundary conditions imposed on both sides. The mesh is extended to 10 chord lengths in all far-field directions.

For the unsteady computations three cycles of motion were computed to obtain periodic solutions. The time variation of the normal force coefficient with respect to the angle of attack on the coarse and fine mesh is given in Fig. 5a for 1000 steps per cycle. As can be observed, the differences between the coarse and fine mesh results are minor, with the fine mesh yielding slightly higher (4%) magnitudes. The effect of time step used on the accuracy of unsteady calculations is illustrated in Fig. 5b. There are again minor differences among the results of cases with 250, 500, and 1000 time steps per cycles of motion, where the slightly higher magnitudes are obtained (5%) with the smallest step size, $\Delta t = 0.051119$ case (1000 steps per cycle). All unsteady solutions are independent of the block subdivision, indicating that the conservation is maintained during parallelization. These results suggest that the Euler solver is reasonably accurate for both mesh sizes and time steps used here, and the finer mesh has a better accuracy. Shown in Fig. 6 is the comparison of the computed normal force coefficient vs the angle-of-attack results with the experimental data of Landon[17] and the Euler solution of Kandil and Chuang[7] for the same case. As

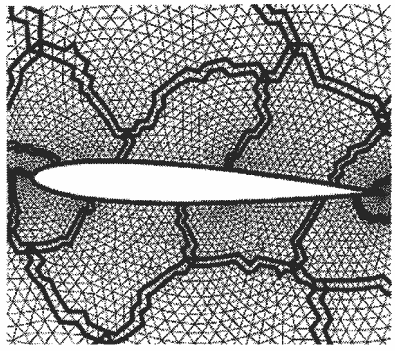

a) At maximum angle-of-attack position

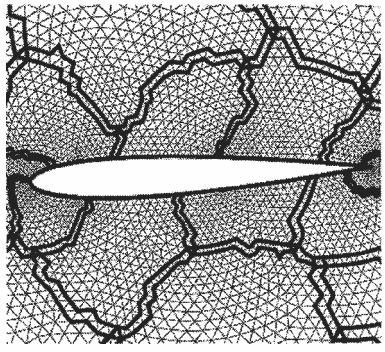

b) At minimum angle-of-attack position

Fig. 4 NACA0012: View of mesh near the airfoil for 20-block model (dark lines indicate overlapping block interfaces).

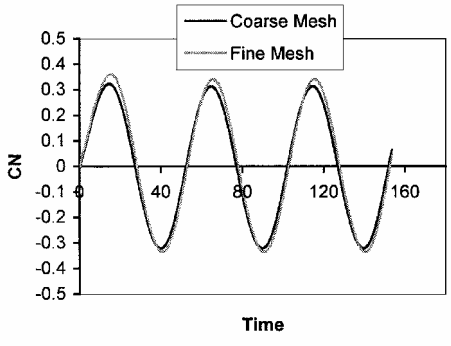

a) Effect of mesh refinement

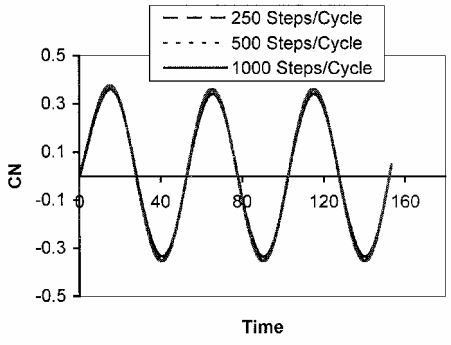

b) Effect of time-step size

Fig. 5 NACA0012: Time variation of normal force coefficient.

can be observed, there is a good agreement with the experiment, in spite of the fact that the viscous effects are neglected in the Euler solver. The comparison of the computed and experimental pressure coefficient values on the airfoil surface is shown in Fig. 7 at the minimum angle-of-attack position $\alpha = -2.41$ deg. These pressure coefficient distributions were taken during the third cycle of the 1000 time steps per cycle of motion computations. As can be observed from these figures, the computed instantaneous pressure coefficient

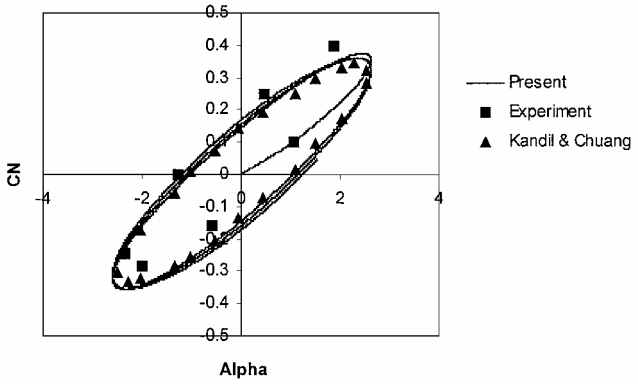

Fig. 6 NACA0012: Variation of normal force coefficient with angle of attack.

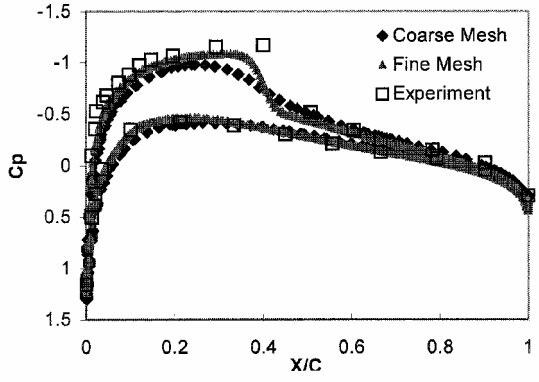

Fig. 7 NACA0012: Pressure coefficient at $\alpha = -2.41$ position.

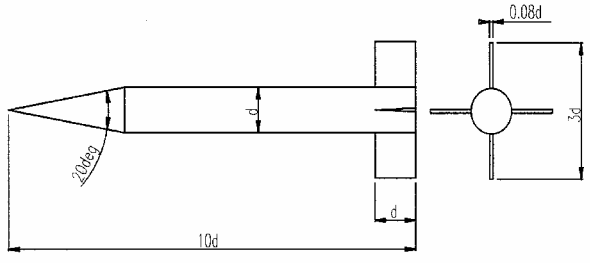

Fig. 8 Basic Finner geometry.[18]

distributions are in good agreement with the experimental pressure coefficient distributions. Furthermore, the difference between the pressure coefficient distributions obtained on the coarse and fine meshes is observed to be reasonable, considering the fact that the coarse mesh has much fewer cells and nodes than the fine mesh.

Missile Case

A missile geometry, commonly known as the Basic Finner,[18] was considered here to demonstrate the various features and the parallel efficiency of the code. The same configuration was analyzed for prediction of the dynamic damping derivatives using the present solver in Ref. 6. Shown in Fig. 8 is the geometry of the Basic Finner. A view of the computational mesh used at zero angle of attack, consisting of 144,216 nodes and 796,105 cells, is shown in Fig. 9. The mesh is extended to $4.5L$ distance in all directions.

The missile was subjected to the sinusoidal pitching oscillations about its center of gravity, $x = 5d$, with the angle-of-attack variation defined in Eq. (15), and $\alpha_m = 0$ deg, $\alpha_p = 10$ deg, $k = 2.53165$, $c = 10d$, and $M_\infty = 1.58$.

The steady-state solution at the mean angle of pitching position was used as an initial solution to the unsteady calculations. The steady-state solution was reached in approximately 300 time steps. Shown in Figs. 10 and 11 are the computational mesh and

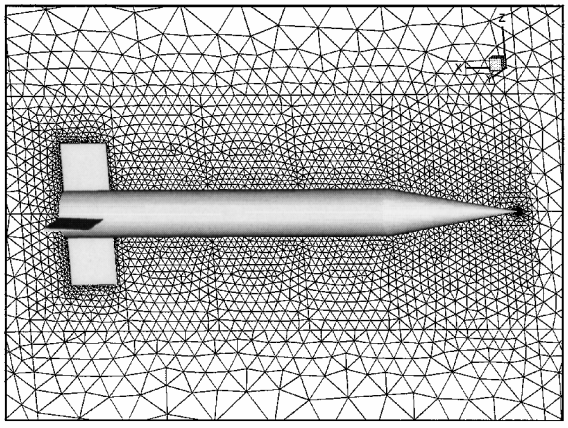

Fig. 9 Basic Finner mesh on the symmetry plane.

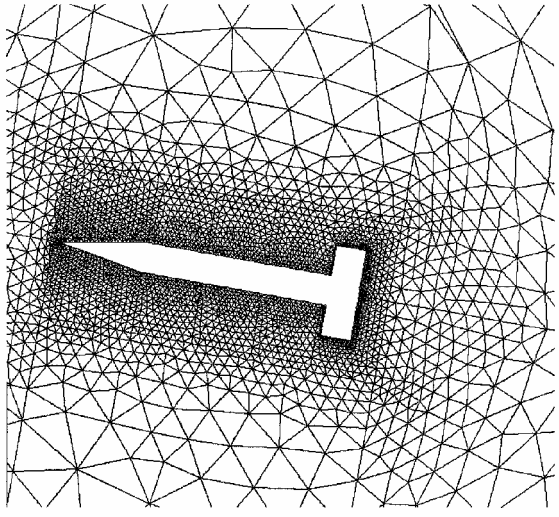

Fig. 10 Basic Finner: Mesh at maximum angle of attack.

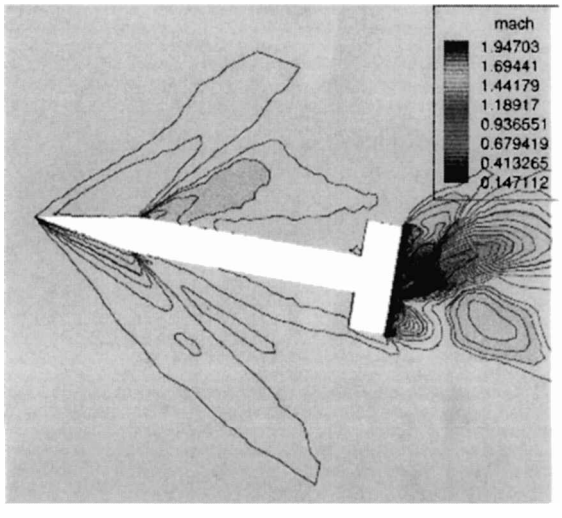

Fig. 11 Basic Finner: Mach contours at maximum angle of attack.

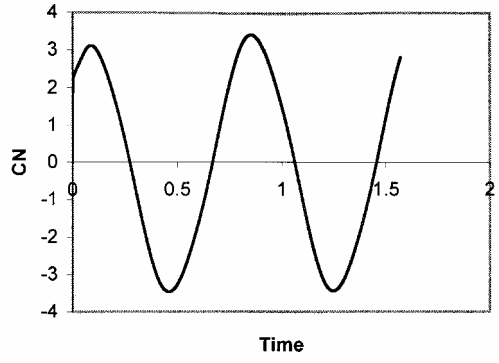

With respect to time

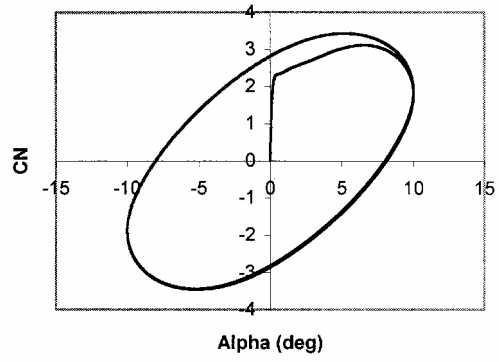

With respect to angle of attack

Fig. 12 Basic Finner: Variation of normal force coefficient.

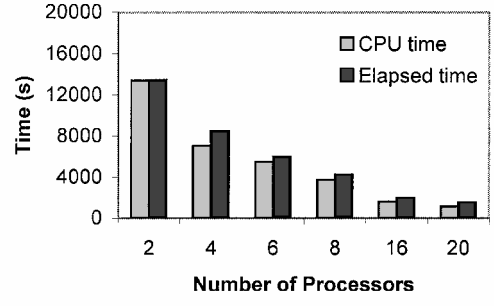

a) Steady solutions

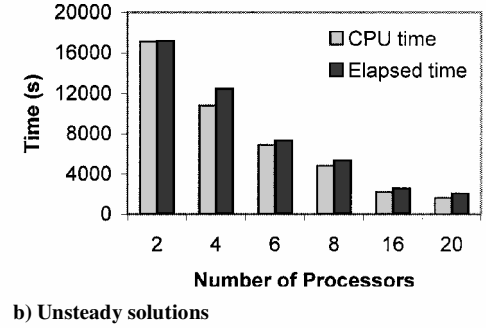

b) Unsteady solutions

Fig. 13 Basic Finner: Comparison of CPU and elapsed times for 200 time steps.

the computed Mach contours, respectively, at the 10-deg angle-of-attack position. The variation of the normal force coefficient for two cycles of motion is shown in Fig. 12. The impulsive transient at the initial time step is caused by sudden start of high frequency oscillations. One cycle of response was computed in 20,000 time steps with $\Delta t = 3.926 \times 10^{-5}$.

CPU and elapsed times were measured to evaluate the parallel performance of the code. Shown in Figs. 13a and 13b are the comparisons of the measured CPU and elapsed times for steady and unsteady cases with different number of processors. Even though the algorithm allows the use of more than one block in a processor, these timings were obtained with one block per processor. The differences between total elapsed and CPU times are caused by communication time needed for exchange of information between the blocks. As can be observed, the CPU and elapsed time requirements of the unsteady solver are higher (about 25%) because of extra computations and communication needed in flow and mesh deformation

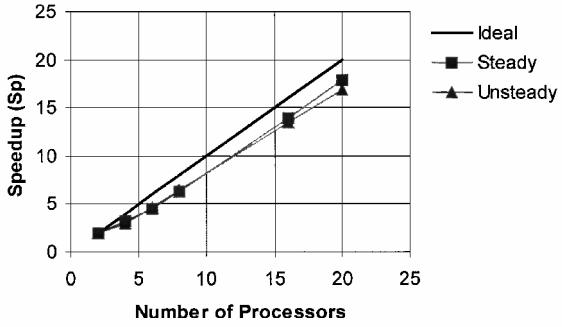

Fig. 14 Basic Finner: Speed up for 200 time steps of steady and unsteady solutions.

algorithms. All of the timings were based on 200 time steps. The parallel speed up of the algorithms for steady and unsteady solutions is summarized in Fig. 14. Here, the speed up is computed from the expression $S_p = T_1/T_p$, where T_1 is the total elapsed time needed to solve the problem with one processor and T_p is the elapsed time needed with p processors. As expected, the speed up for the unsteady case is slightly lower than the steady solution case. For the mesh and the computer system used here, the steady solver is 90% efficient with 20 processors, while the unsteady solver is 85% efficient, where the percent efficiency defined as $E = 100 \times S_p/p$.

Conclusions

In this research the serial and steady flow version of the computer program USER3D has been modified and parallelized for the solution of steady and unsteady Euler equations on unstructured meshes. A deforming mesh approach is used for unsteady movements of bodies. The solution algorithm was based on a finite volume method with an implicit time-integration scheme. Parallelization was based on a domain-decomposition approach and the message passing between the parallel processes was achieved using the MPI[15] message passing library for parallel computing. Several steady and unsteady problems were analyzed to demonstrate the possible applications of the current solution method. Reasonable efficiencies were achieved for up to 20 processors while solving both steady and unsteady flows. The features of the algorithms presented here can be cited as follows: 1) a three-dimensional unstructured solver with arbitrary partitions suitable for complex geometries, 2) ability for arbitrary mesh deformations allows accurate unsteady solution of moving body problems, 3) both flow and deforming mesh algorithms are parallelized, 4) ability for multiprocessing on heterogeneous systems by assigning one or more partitions to each processor is suitable for load balancing on heterogeneous systems, and 5) fast and time-accurate computations. Practical applications of the tools developed here can be found in Ref. 6 for determination of dynamic stability derivatives, such as pitch and roll damping, needed for missile design.

Acknowledgments

The authors express their appreciation to Zhenyin Li of the Indiana University—Purdue University Indianapolis CFD Laboratory for the expert assistance provided in performing the computer runs needed for this paper. The computer support was provided on the CFD Laboratory's local and wide area networks by Resat Payli; and the computer access provided on the Indiana University's IBM SP system by the University Information Technology Services (UITS) are gratefully acknowledged.

References

[1]Uzun, A., Akay, H. U., and Bronnenberg, C., "Parallel Computations of Unsteady Euler Equations on Dynamically Deforming Unstructured Grids," *Proceedings of Parallel CFD'99*, edited by D. Keyes, A. Ecer, N. Satofuka, and J. Periaux, Elsevier Science, Amsterdam, 2000, pp. 415–422.

[2]Oktay, E., "USER3D, 3-Dimensional Unstructured Euler Solver," ROKETSAN Missile Industries Inc., SA-RS-RP-R 009/442, Ankara, Turkey, May 1994.

[3]Oktay, E., Alemdaroğlu, N., Tarhan, E., Champigny, P., and d'Espiney, P., "Euler and Navier–Stokes Solutions for Missiles at High Angles of Attack," *Journal of Spacecraft and Rockets*, Vol. 36, No. 6, 1999, pp. 850–858.

[4]Oktay, E., and Asma, C. O., "Drag Prediction with an Euler Solver at Supersonic Speeds," *Journal of Spacecraft and Rockets*, Vol. 37, No. 5, 2000, pp. 692–697.

[5]Roe, P. L., "Characteristic-Based Schemes for the Euler Equations," *Annual Review of Fluid Mechanics*, Vol. 18, 1986, pp. 337–365.

[6]Oktay, E., and Akay, H. U., "CFD Predictions of Dynamic Derivatives for Missiles," AIAA Paper 2002-0276, Jan. 2002.

[7]Kandil, O. A., and Chuang, H. A., "Computation of Steady and Unsteady Vortex-Dominated Flows with Shock Waves," *AIAA Journal*, Vol. 26, No. 5, 1988, pp. 524–531.

[8]Trepanier, J. Y., Reggio, M., Zhang, H., and Camarero, R., "A Finite Volume Method for the Euler Equations on Arbitrary Lagrangian-Eulerian Grids," *Computers and Fluids*, Vol. 20, No. 4, 1991, pp. 399–409.

[9]Benek, J. A., Buning, P. G., and Steger, J. L., "A 3D Chimera Grid Embedding Technique," AIAA Paper 85-1523, July 1985.

[10]Singh, K. P., Newman, J. C., and Baysal, O., "Dynamic Unstructured Method for Flows Past Multiple Objects in Relative Motion," *AIAA Journal*, Vol. 33, No. 4, 1995, pp. 641–649.

[11]Frink, N. T., Parikh, P., and Pirzadeh, S., "A Fast Upwind Solver for the Euler Equations on Three-Dimensional Unstructured Meshes," AIAA Paper 91-0102, Jan. 1991.

[12]Batina, J. T., "Unsteady Euler Algorithm with Unstructured Dynamic Mesh for Complex Aircraft Aerodynamic Analysis," *AIAA Journal*, Vol. 29, No. 3, 1991, pp. 327–333.

[13]Anderson, W. K., "Grid Generation and Flow Solution Method for Euler Equations on Unstructured Grids," *Journal of Computational Physics*, Vol. 11, No. 1, 1994, pp. 23–38.

[14]Akay, H. U., Blech, R., Ecer, A., Ercoskun, D., Kemle, B., Quealy, A., and Williams, A., "A Database Management System for Parallel Processing of CFD Algorithms," *Proceedings of Parallel CFD '92*, edited by R. B. Pelz, A. Ecer, and J. Hauser, Elsevier Science, Amsterdam, 1993, pp. 9–23.

[15]"MPI: A Message Passing Interface Standard—Message Passing Interface Forum," *The International Journal of Supercomputer Applications and High Performance Computing*, Vol. 8, Nos. 3–4, 1994.

[16]Bronnenberg, C. E., "GD: A General Divider User's Manual—An Unstructured Grid Partitioning Program," CFD Lab., Indiana Univ.—Purdue Univ. Indianapolis, Rept. 99-01, Indianapolis, IN, June 1999.

[17]Landon, R. H., "NACA 0012. Oscillating and Transient Pitching," *Compendium of Unsteady Aerodynamic Measurements, Data Set 3*, AGARD-R-702, London, Aug. 1982.

[18]Shantz, I., and Groves, R. T., "Dynamic and Static Stability Measurements of the Basic Finner at Supersonic Speeds," NAVORD, Rept. 4516, Whiteoak, MD, Jan. 1960.